

Unusual evolution from a superconducting to an antiferromagnetic ground state in $Y_{1-x}Gd_xPb_3$ ($0 \leq x \leq 1$)

M. Cabrera-Baez,^{1,*} V. C. Denis,² L. Mendonça-Ferreira,² M. Carlone,³ P. A. Venegas,⁴ M. A. Avila,² and C. Rettori^{1,2}

¹Instituto de Física “Gleb Wataghin,” UNICAMP, Campinas, São Paulo 13083-859, Brazil

²CCNH, Universidade Federal do ABC, Santo André, São Paulo 09210-580, Brazil

³Programa de Pós-Graduação em Ciência e Tecnologia de Materiais, Faculdade de Ciências, Universidade Estadual Paulista - UNESP, Bauru, São Paulo 17033-360, Brazil

⁴Departamento de Física, Faculdade de Ciências, Universidade Estadual Paulista, Bauru, São Paulo 17033-360, Brazil



(Received 21 February 2018; revised manuscript received 16 May 2018; published 22 June 2018)

We have studied the evolution of $Y_{1-x}Gd_xPb_3$ ($0 \leq x \leq 1$) from its superconducting ($x = 0$) to antiferromagnetic ($x = 1$) states with critical temperatures $T_c = 4.6(2)$ K and $T_N = 15.7(2)$ K, respectively. At relatively low Gd concentrations ($x \leq 0.03$) T_c presents a weak but linear suppression with increasing x , as expected from the Abrikosov-Gorkov (AG) theory describing the Cooper pair breaking due to the exchange interaction between the impurity localized magnetic moment and the conduction electrons (ce). This linear T_c suppression rate leads to an effective exchange parameter of $\langle J^2(\mathbf{q}) \rangle_{AG}^{1/2} = 0.20(7)$ meV between the $4f$ localized electrons and the ce . For intermediate Gd concentrations ($0.03 \leq x \leq 0.15$), although no Gd clustering is observed, there is an unusual inflection and leveling off trend in T_c , indicating that the superconducting phase persists until the highest Gd concentration in this region where magnetic interactions are evidenced by increasingly negative values of the Curie-Weiss temperature Θ_C . Analysis of low- T Gd^{3+} electron spin resonance (ESR) experiments and their ESR line-shape simulations, in conjunction with the trend in T_c , leads us to suggest that an exchange bottleneck mechanism between the Gd^{3+} localized magnetic moment and the ce may be the reason behind the inhibition of the Cooper pair-breaking mechanism, in favor of a magnetic interaction via ce polarization. Therefore, our superconducting and ESR results suggest a scenario where superconducting and magnetic phases coexist extensively in the $Y_{1-x}Gd_xPb_3$ system, mediated by different types of ce .

DOI: [10.1103/PhysRevB.97.224425](https://doi.org/10.1103/PhysRevB.97.224425)

I. INTRODUCTION

Intermetallic compounds of the family RX_3 ($R =$ rare earth, $X =$ In, Sn, Tl, and Pb) with $AuCu_3$ structure (space group $Pm\bar{3}m$) have long attracted attention due to their interesting physical properties and relatively easy modeling. Magnetism, superconductivity, heavy-fermion behavior, and other unusual electronic ground states are a few examples of the richness in this family of compounds [1–3]. $LaSn_3$ and YSn_3 are examples of relatively high T_c superconductors within this family [4–6], with $T_c = 6.25$ K and $T_c = 7.0$ K, respectively, in contrast to $CaPb_3$, YIn_3 , $LaIn_3$, $YbPb_3$, and $ThTl_3$ which were reported as superconductors with T_c lower than 1 K [6]. With respect to magnetic ordering, $SmPb_3$ was reported to be an antiferromagnetic material with $T_N = 5$ K [7], whereas $GdPb_3$ is antiferromagnetic below 17 K [8]. Evidence of dense Kondo effects and the presence of heavy electrons was reported in $PrSn_3$ [9]. Additionally, the family has proved a favorable one for gradual substitution of one element by another as a control parameter, maintaining the same phase, which allows us to track the evolution of ground states and the interplay of its main interactions. As such, this family of compounds offers the opportunity to explore interesting physical behaviors, in particular, superconductivity, magnetism, and their coexistence.

Low concentrations of localized magnetic moments (LMMs) in a superconductor have been modeled theoretically by Abrikosov and Gorkov (AG) [10]. According to this formalism, the addition of rare-earth impurities leads to strong suppression of T_c with typical critical concentrations of about $x = 0.01$, demonstrating the antagonism between magnetism and superconductivity. Among the so-called conventional superconductors $LaSn_3$ is one practical example [11], as confirmed by the addition of a small Gd substitution ($La_{1-x}Gd_xSn_3$). Similarly, the RNi_2B_2C ($R = Y, Lu$) compounds were classified as conventional BCS superconductors [12]. Particularly, in the RPb_3 family of compounds it seemed instructive to take advantage of the superconductivity in YPb_3 and antiferromagnetism in $GdPb_3$, following the evolution of the Cooper pair breaking as Gd is gradually added to the superconducting compound and therefore probing the degree of conventionality.

Electron spin resonance (ESR) of rare-earth ions [13] both diluted and concentrated in intermetallic materials has been largely used as a local technique to investigate the microscopic properties of elemental [14], correlated electron systems [15], superconducting materials [11,12], and topological insulators [16], among others, since it directly probes LMMs and the nature of the involved interactions with their surroundings [17–19]. The ESR technique applied to superconducting materials such as the present case of YPb_3 doped with Gd^{3+} gives important information, mainly extracted from the line shape

*mcabrera@ifi.unicamp.br

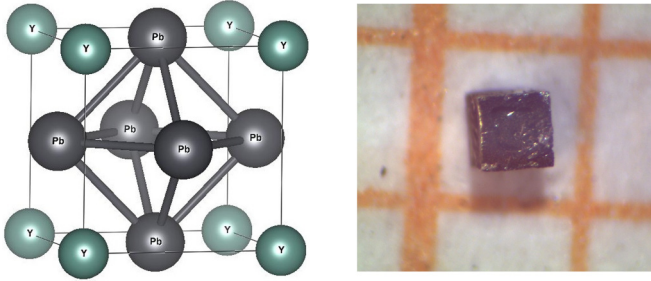


FIG. 1. (left) Representation of the cubic unit cell of YPb_3 ($a \approx 4.8 \text{ \AA}$) and (right) photo of a typical cubic-shaped single crystal of YPb_3 on millimeter paper.

as the linewidth ΔH related to spin-lattice relaxation and the resonance field H_{res} related to the g shift. Both parameters are proportional to the exchange interaction between the LMMs and ce , J_{f-ce} , and can be compared with the Cooper pair breaking predicted from AG theory due to the exchange between Gd^{3+} and ce .

This work aims to explore the evolution from superconductivity to magnetism for a wide range of Gd concentrations in the $\text{Y}_{1-x}\text{Gd}_x\text{Pb}_3$ system. Our main results show the existence of three different regimes as a function of the Gd^{3+} doping: (i) low concentration ($x \leq 0.03$) dominated by a narrowing of the Gd^{3+} ESR fine structure via the Korringa relaxation mechanism (crystal field effects and exchange coupling between a $4f$ localized magnetic moment and the ce), (ii) an intermediate region ($0.03 \leq x \leq 0.15$) dominated by the competition between the $4f-ce$ and $4f-4f$ interactions in agreement with the Hasegawa-Korringa model [20] for the spin-lattice relaxation, and (iii) a high-concentration regime ($x = 0.15, 0.34, 1.0$), characterized by only the $4f-4f$ interaction, as expected for an antiferromagnetic system. With the support of density functional theory (DFT) band structure calculations, we conclude that superconductivity and magnetism are principally mediated by different types of ce in this system: s -type ce should be responsible for the superconductivity and the p or d type of ce should mediate the Gd-Gd antiferromagnetic coupling.

II. EXPERIMENTAL DETAILS

Single crystals of $\text{Y}_{1-x}\text{Gd}_x\text{Pb}_3$ ($0 \leq x \leq 1$) were grown out of excess Pb using a standard self-flux method [21,22]. The constituent elements were 99.9% pure Y, Gd, and 99.9% pure Pb. The initial ratios of the starting elements were $1-x : x : 32$, sealed inside evacuated quartz ampoules. The tubes were heated and kept at a temperature of 1100°C for 3 h. Then crystals were grown by slowly cooling the melt between 1100°C and 500°C over 150 h. At 500°C the ampoules were removed from the furnace, inverted, and placed in a centrifuge to spin off the excess Pb flux. The individual crystals were typically cubes of $\sim 1 \text{ mm}^3$ in size (Fig. 1).

Powder x-ray diffraction (XRD) at room T on finely crushed crystals was performed on a Bruker D2 Phaser AXS to confirm the crystal structure and phase purity. The effective Gd concentrations x on all samples were estimated using energy dispersive x-ray spectroscopy measurements in a JEOL JSM-6010LA scanning electron microscope with a Vantage

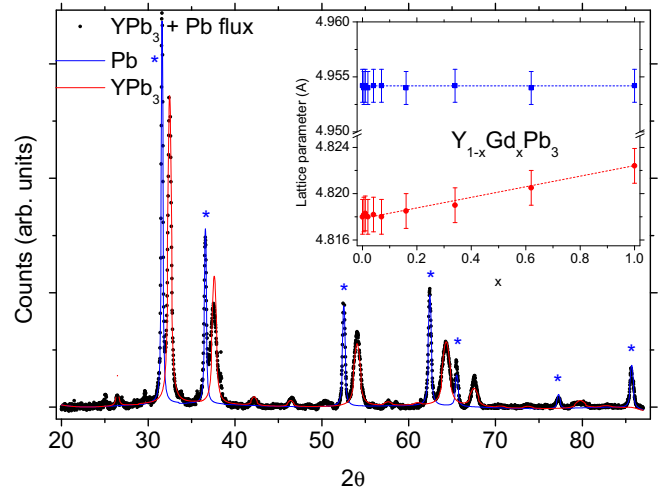


FIG. 2. X-ray diffraction pattern of powdered YPb_3 crystals showing peaks for the pure phase and for attached Pb flux. The inset shows the evolution of the lattice parameter of YPb_3 corresponding to the expected expansion of the unit cell, while the lattice parameter for Pb flux remains unchanged within experimental precision.

energy dispersive spectroscopy (EDS) system. The obtained values are in good agreement with those extracted from dc magnetic susceptibility, assuming the free-ion magnetic moment of Gd^{3+} ($\mu_B = 7.94\mu_B$). The dc magnetic susceptibility ($\chi = M/H$) measurements were conducted on a Quantum Design MPMS3 magnetometer [superconducting quantum interference device (SQUID)–vibrating-sample magnetometer] under applied fields $H \leq 30 \text{ kOe}$ and temperatures in the interval $2.0 \text{ K} \leq T \leq 310 \text{ K}$. For the ESR experiments, single crystals were crushed, and powder samples were prepared by selecting particles with sizes greater than $100 \mu\text{m}$, corresponding to average grain size d larger than the skin depth δ , $\lambda = d/\delta \gtrsim 10$. The X-band ($\nu \approx 9.4 \text{ GHz}$) ESR experiments were carried out in a conventional cw Bruker-ELEXSYS 500 ESR spectrometer using a TE_{102} cavity. The sample temperature was changed by using a helium gas flux coupled to an Oxford temperature controller.

III. EXPERIMENTAL RESULTS

We first verify that $\text{Y}_{1-x}\text{Gd}_x\text{Pb}_3$ maintains a consistent crystallographic structure throughout the substitution range. Figure 2 displays the room- T XRD pattern of powdered YPb_3 single crystals as well as that of the simulated structure (solid red line). The observed reflections were identified as the expected cubic AuCu_3 -type structure for YPb_3 with lattice parameter $a = 4.818(2) \text{ \AA}$ (red line), in agreement with previous results [2]. The additional peaks marked by asterisks are indexed as cubic Pb with $a = 4.9542(2) \text{ \AA}$ (blue line) [23]. It is worth mentioning that excess Pb flux was found to be difficult to remove completely from the flux-grown crystals, and some amount inevitably remained present on the surfaces (see Fig. 3) and trapped within the crystal cubes. Nevertheless, as will be discussed below, this will not affect the analysis of the data and interpretation of our main results. The inset of Fig. 2 shows the evolution of the lattice parameters as a

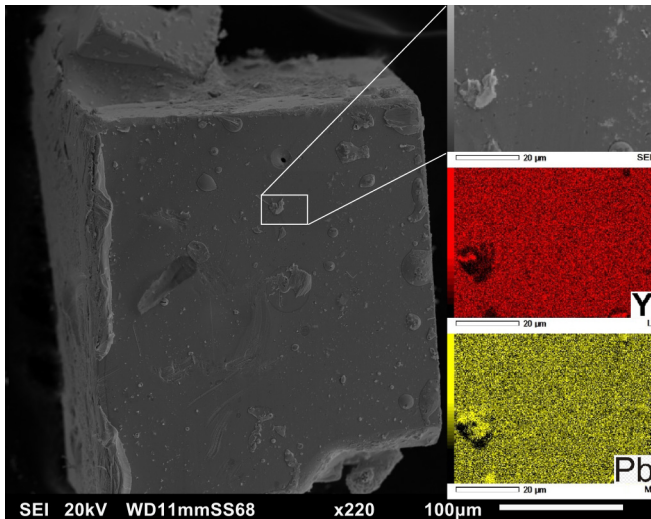


FIG. 3. SEM image of $Y_{0.93}Gd_{0.07}Pb_3$ with a map of the distribution and relative proportion (intensity) of Y (red) and Pb (yellow) over the scanned area.

function of Gd content, both for $Y_{1-x}Gd_xPb_3$ with $0 \leq x \leq 1$ and for cubic Pb. A linear increase for $Y_{1-x}Gd_xPb_3$ with the Gd substitution is observed, as expected from Vegard's law for a solid solution. Notice that, within the uncertainty of the measurements, the lattice parameter of the cubic Pb remains constant, indicating the absence of any significant amount of Gd in the flux.

The next important characterization step is to check for excess Pb and/or possible clustering of Gd ions as they enter the YPb_3 matrix. Figure 3 shows a scanning electron microscope (SEM) image of a $Y_{0.93}Gd_{0.07}Pb_3$ single crystal, including the mappings of Y and Pb distributions with a relative proportion (intensity) in a selected area. Small Pb flux droplets attached to the surface are seen. Although it was not possible to map the precise Gd distribution because of its small amount, EDS analysis of the Gd concentration evaluated at several crystal points matches the expected nominal x of Gd in each sample. The collective SEM data set evidences homogeneous solid solutions within the full range of crystal compositions.

Having established the crystal qualities, we proceed to the magnetic characterization. The dc magnetization of the pure crystal as a function of temperature and different applied magnetic fields is presented in Fig. 4. The inset highlights the curve for $H = 20$ Oe, where two transitions can be distinguished, one at $T_c = 4.6(2)$ K corresponding to the YPb_3 superconducting transition [24] and a second at $T_c = 7.1(2)$ K associated with that of cubic Pb [25]. Increasing applied fields lead to stronger diamagnetism and suppression of both transitions, as expected.

Figure 5 shows the magnetic-field-temperature (H vs T) phase diagram built from the magnetic measurements performed on the pure YPb_3 single crystal. The lower critical field H_{c1} has been estimated from magnetization hysteresis loops (M vs H) at various temperatures (see inset), identified as the deviation point from linear Meissner behavior, as indicated in the figure. Due to the presence of Pb flux in our samples, which contributes an additional diamagnetic signal at higher

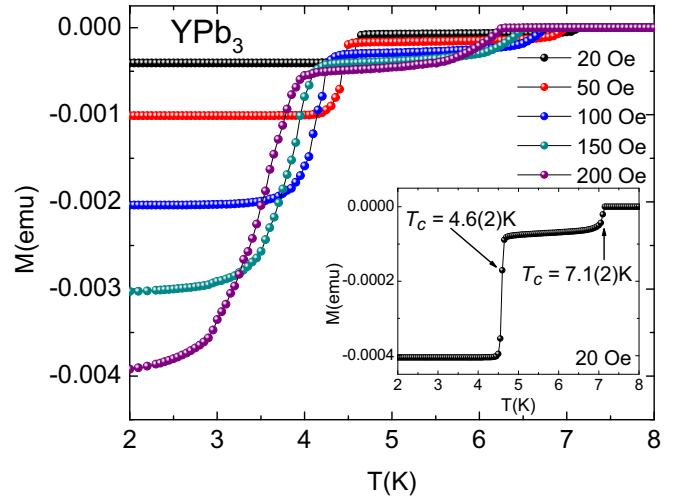


FIG. 4. The dc magnetization as a function of temperature for YPb_3 under different applied magnetic fields. The inset shows an expanded view of the curve for 20 Oe.

fields, we could not clearly identify the upper critical field H_{c2} from the M vs H curves. Hence, we tentatively estimated H_{c2} from the T -dependent zero-field-cooled magnetization curves measured at various fields. In this case, we identified the critical temperature at a given magnetic field as the temperature of the maximum in the corresponding derivative curve. Due to the broadening of the superconducting transition induced by the applied magnetic field, this procedure was restricted to samples with lower Gd concentrations.

With the basic magnetic response of our YPb_3 crystals determined, we begin tracking the effects of Gd doping. Figure 6 shows the evolution of the superconducting critical temperature measured from dc magnetic susceptibility at $H = 20$ Oe as a function of the Gd content ($Y_{1-x}Gd_xPb_3$; $0 \leq x \leq 0.16$). The data present a weak linear decrease of T_c (0.31

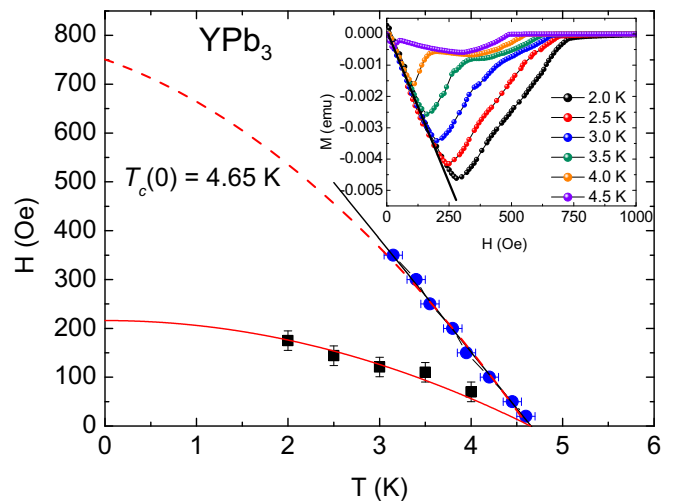


FIG. 5. Lower critical field H_{c1} and upper critical field H_{c2} as a function of temperature for YPb_3 . The solid red line represents the fitting of the equation $H_{c1}(T) = H_{c1}(0)[1 - (T/T_c)^2]$. The dashed red line represents a free extrapolation based on the WHH calculation of $H_{c2}(0) = 773(20)$ Oe (see text).

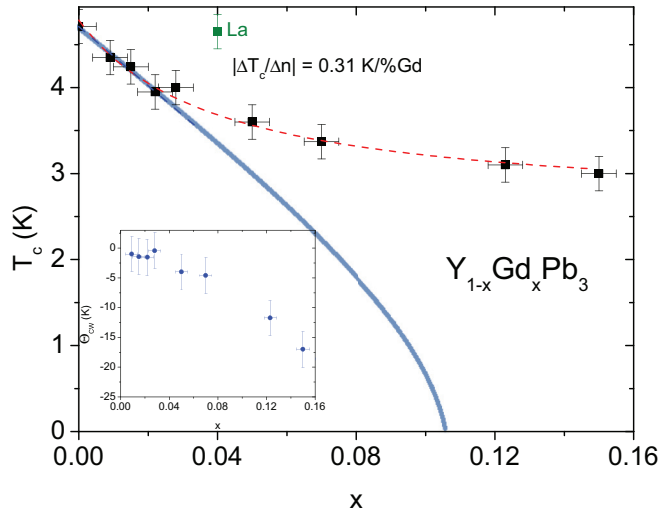


FIG. 6. Evolution of the superconducting temperature T_c as a function of Gd content (x of Gd) in the case of $Y_{1-x}Gd_xPb_3$ with $0 \leq x \leq 0.16$ compared with the AG trend (blue line). The inset shows the associated value of the Curie-Weiss temperature extracted from dc magnetic susceptibility measurements.

K/%Gd) for low Gd concentrations (up to $x \lesssim 0.03$), similar to the initial trend of the AG function (blue solid line), followed by an unusual deviation from this function (red dashed line) characterized by a leveling off trend at higher concentrations ($0.02 \lesssim x \lesssim 0.15$). The inset of Fig. 6 presents the Curie-Weiss temperature Θ_{CW} as a function of Gd content. Notice the increase in magnitude of Θ_{CW} above $x \sim 0.05$, reaching $\Theta_{CW} = -17.5$ K even for samples with superconducting temperatures of $T_c \approx 3$ K. Also included in Fig. 6 is the T_c of a La-substituted sample ($La_{0.04}Y_{0.96}Pb_3$, green data point in the main graph), which shows no significant change compared to pure YPb_3 , indicating that negative chemical pressure effects due to the difference in the ionic radius between Y^{3+} and Gd^{3+}

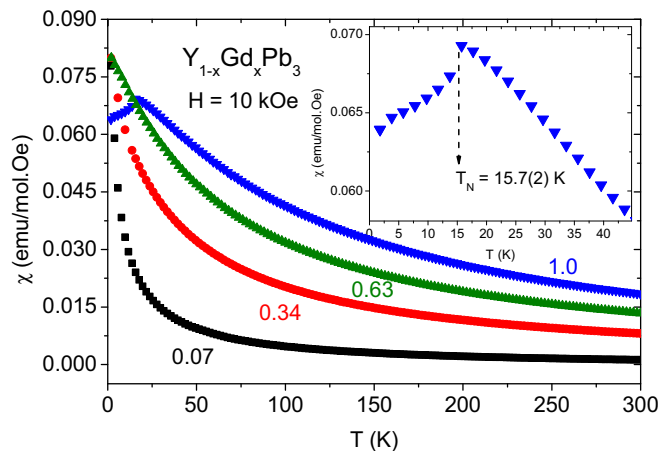


FIG. 7. T dependence of the dc magnetic susceptibility χ of $Y_{1-x}Gd_xPb_3$ for $x = 0.07, 0.34, 0.63,$ and 1.0 at $H = 10$ kOe. The inset zooms in on the low- T antiferromagnetic transition at $T_N = 15.7(2)$ K for $x = 1.0$.

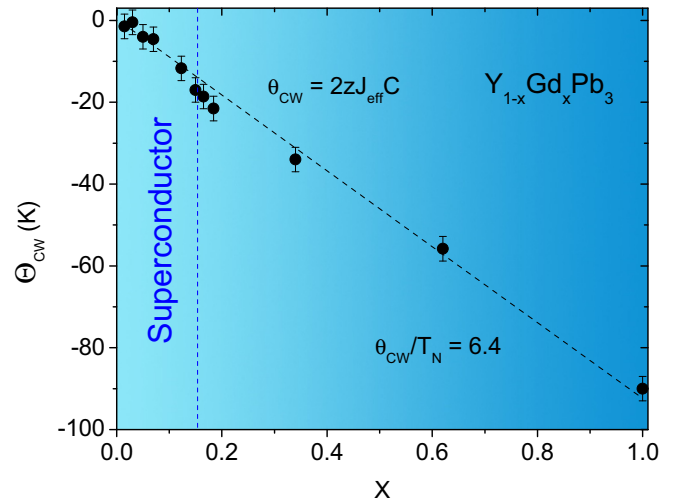


FIG. 8. Gd concentration dependence of the Curie-Weiss temperature of $Y_{1-x}Gd_xPb_3$ in the full range, $0 \leq x \leq 1$.

ions should be irrelevant, and any suppression of T_c caused by Gd substitution should, indeed, be magnetic in origin.

Figure 7 presents the T dependence of the magnetic susceptibility of $Y_{1-x}Gd_xPb_3$ for $x = 0.07, 0.34, 0.63,$ and 1.0 , the latter (pure $GdPb_3$) showing an antiferromagnetic transition at $T_N = 15.7(2)$ K (see inset). Several other concentrations were measured but are not shown here for clarity. Fitting the Curie-Weiss law between 100 and 300 K leads to Gd^{3+} concentrations close to the nominal values, assuming the effective magnetic moment of $\mu_{eff} = 7.94\mu_B/f.u.$ expected for Gd^{3+} ions. The fits for all measured samples also provide the respective Curie-Weiss temperatures Θ_{CW} , plotted in Fig. 8 as a function of Gd concentration x . Above $x \sim 0.03$ there is a smooth, linear evolution, reaching large negative values and ending at $\Theta_{CW}/T_N = 6.4$ for pure $GdPb_3$.

In order to explore the microscopic effects of adding Gd^{3+} ions to YPb_3 , ESR experiments were performed on all samples, and strikingly different behaviors were observed for different levels of Gd concentration. Figure 9 shows the typical Gd^{3+} ESR lines at different temperatures ($4.5 \text{ K} \leq T \leq 9.8 \text{ K}$) for low-concentration samples such as $Y_{0.985}Gd_{0.015}Pb_3$. Notice that the linewidth from the line-shape analysis tends to *narrow* as the temperature increases (see inset of Fig. 9), contrary to what was observed in analogous experiments for Gd-doped YIn_3 [26]. For intermediate Gd concentration $x \sim 0.045$ to $x \sim 0.15$ (see Fig. 10) the ESR lines become almost T independent, and for high concentration, above 0.15 (Fig. 10), the ESR lines broaden at low T , evidencing Gd-Gd interaction. The red lines in both graphs represent the simulations, which will be discussed in the next section.

IV. ANALYSIS AND DISCUSSION

As shown in Fig. 1, YPb_3 presents a cubic unit cell with $a = 4.818(2)$ Å, manifested in the morphology of the as-grown single crystals with sizes smaller than 1 mm. The expected cubic phase was confirmed by XRD experiments (Fig. 2) that, however, inevitably show the presence of the cubic Pb coming from the excess flux. The Pb flux was removed as carefully as

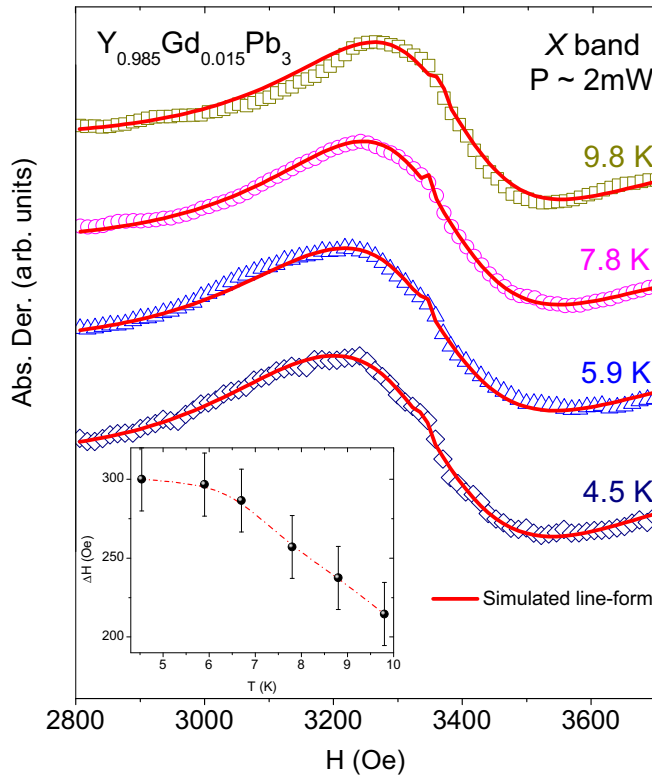


FIG. 9. X-band Gd^{3+} ESR spectra in $\text{Y}_{0.985}\text{Gd}_{0.015}\text{Pb}_3$ at different temperatures and a microwave power of 2 mW. The solid red lines represent the simulated line forms. The inset shows the linewidth evolution with temperature.

possible from the crystal surfaces, but SEM images of crushed crystals still revealed a small amount of it inside the crystals. Thus, our first concern was whether Gd might be incorporated in the cubic lattice of the Pb flux, which could result in unwanted contributions to the resonance signals in the ESR experiments. However, the inset of Fig. 2 shows no detectable change in the Pb flux cubic lattice parameter by the addition of Gd atoms, contrary to what one may expect from Vegard's law for $\text{Pb}_{1-x}\text{Gd}_x$. As further confirmation, the inset of Fig. 4 shows that the Pb flux superconducting transition temperature is $T_c = 7.1(2)$, the same as that of pure Pb, and remains the same for all Gd concentrations. The above discussion allows us to ignore any possible presence of Gd ions left in Pb and focus only on the ESR of Gd^{3+} in $\text{Y}_{1-x}\text{Gd}_x\text{Pb}_3$ ($0 \leq x \leq 1$).

The magnetization experiments under different applied magnetic fields on YPb_3 allow the estimation of important superconducting parameters. The solid red curve in the phase diagram for YPb_3 (see Fig. 5) is a fitting to the mean-field equation $H_{c1}(T) = H_{c1}(0)[1 - (T/T_{c0})^2]$, where $H_{c1}(0)$ is the lower critical field at absolute-zero temperature and T_{c0} is the superconducting critical temperature at zero magnetic field, giving $H_{c1}(0) = 216(9)$ Oe. As can be seen in Fig. 5, the upper critical field follows a linear dependence on T at higher temperatures with a rate of $dH_{c2}(T)/dT = -231(6)$ Oe/K. This enables us to calculate the orbital limiting field at absolute zero given by the Werthamer-Helfand-Hohenberg (WHH) theory [27] for dirty type-II superconductors, $H_{c2}(0) = -0.70T_{c0}[dH_{c2}(T)/dT]$. The value found,

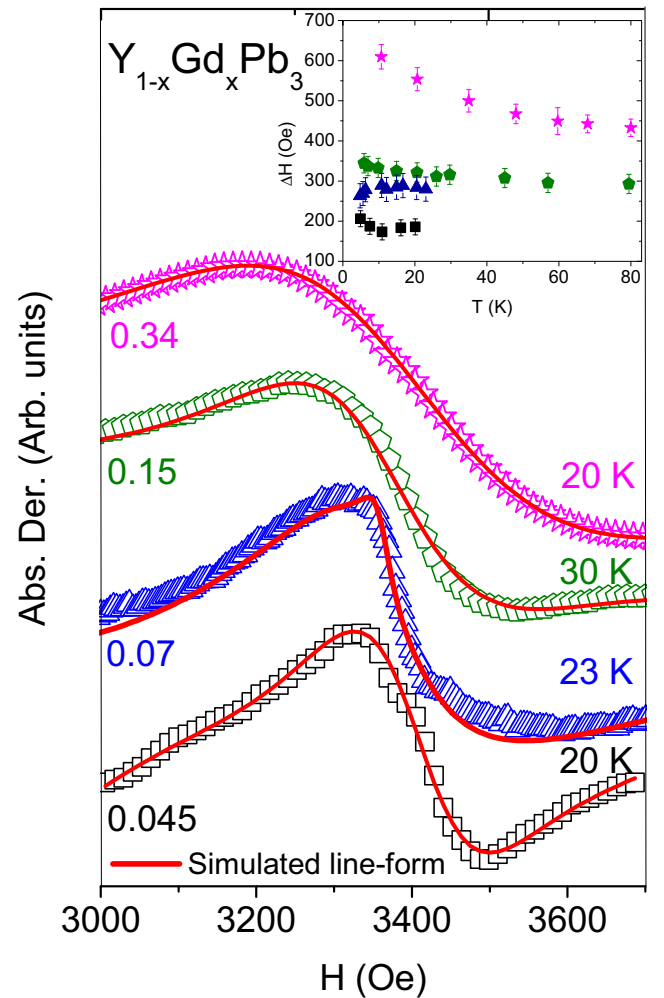


FIG. 10. X-band Gd^{3+} ESR spectra in $\text{Y}_{1-x}\text{Gd}_x\text{Pb}_3$ for $x = 0.045, 0.07, 0.15,$ and 0.34 . The solid red lines represent the simulated line forms. The inset shows the linewidth dependence on temperature for $x = 0.07, 0.15,$ and 0.34 .

$H_{c2}(0) = 750(20)$, Oe is largely surpassed by the paramagnetic or Pauli limiting field $H_p = 86000$ Oe calculated from [28], $H_p = \delta_0/(2)^{1/2}\mu_B$, where δ_0 is the zero-temperature value of the superconducting gap, μ_B is the Bohr magneton, and, assuming the well-known relation for a BCS superconductor, $\delta_0 = 1.76k_B T_{c0}$. Hence, our results give a Maki parameter [29] $\kappa_M = \sqrt{2}H_{c2}(0)/H_p = 0.012$ that in most superconductors is usually much less than unity, indicating that pair breaking due to paramagnetic effects is negligible in YPb_3 . This important result is in complete agreement with the observed extended region of coexistence between superconductivity and magnetism adding magnetic Gd impurities to the system.

The coherence length at $T = 0$, ξ_0 , was estimated from the Ginzburg-Landau relation $H_{c2}(0) = \phi_0/(2\pi\xi_0^2)$, where $\phi_0 = 2.0678 \times 10^9$ Oe \AA^2 is the magnetic flux quantum [30]. Both critical fields are related to the thermodynamic critical field through $H_c = (H_{c1}H_{c2})^{1/2}$. From this we calculate the dimensionless Ginzburg-Landau parameter κ , using $H_{c2}(0) = 2^{1/2}\kappa H_c(0)$, whereby the resulting value of $1.32 > 1/2^{1/2}$ implies type-II superconductivity for YPb_3 . Finally, the London

TABLE I. Characteristic superconducting parameters obtained for $Y_{1-x}Gd_xPb_3$.

x	$T_c(0)$	$H_{c1}(0)$ (Oe)	$H_{c2}(0)$ (Oe)	H_c (Oe)	ξ_0 (Å)	λ_0 (Å)	κ
0	4.65	216(9)	750(20)	402	662	874	1.32
0.015	4.26	193(9)	470(20)	301	838	922	1.10
0.017	4.24	136(5)	230(20)	179	1196	1076	0.90

penetration depth was calculated from the relation $\lambda_0 = \kappa_0 \xi_0$, giving 874 Å. Table I presents the same parameters determined in a similar manner for some Gd-doped samples. A reduction of some superconducting parameters is observed [T_c , $H_{c1}(0)$, $H_{c2}(0)$, and $H_c(0)$] when the Gd concentration x increases in the system. This is expected since Gd^{3+} favors the Cooper pair-breaking effect, which becomes less superconducting. However, conversely, the coherence length ξ_0 and the London penetration depth λ_0 increase with x , also facilitating the penetration of the external magnetic field.

The effect of the Gd ions on the superconducting temperature T_c of $Y_{1-x}Gd_xPb_3$ for $0 \leq x \leq 0.15$ is shown in Fig. 6, where an unusual extended region of coexistence between superconductivity and magnetism is observed. The initial linear decrease in the superconducting temperature ($0 \leq x \leq 0.03$) follows the AG theory. Although this theory successfully explained the linear reduction of T_c with increasing magnetic impurities, some important assumptions were made in the AG formalism. One of those is the requirement of randomly distributed impurities with no magnetic interactions between them, i.e., the absence of magnetic clusters. This condition is usually well obeyed for low concentrations of a solid solution, as in our case for the interval $0 \leq x \leq 0.03$ in $Y_{1-x}Gd_xPb_3$. Hence, it is possible to use the simplified expression for the Cooper pair-breaking effect in the superconducting state due to the presence of magnetic impurities as follows:

$$\left| \frac{\Delta T_c}{\Delta x} \right| = \frac{\pi^2}{8k_B} \langle J_{f,ce}^2(\mathbf{q}) \rangle \eta_F (g_J - 1)^2 J(J+1) \quad (1)$$

Here, $\langle J_{f,ce}^2(\mathbf{q}) \rangle$ is the square of the effective exchange interaction between the local $4f$ magnetic moment and the ce in the presence of momentum transfer averaged over the whole Fermi surface, η_F is the “bare” density of states for one spin direction at the Fermi level, and $(g_J - 1)^2 J(J+1)$ is the de Gennes factor, which for Gd is given by $S(S+1)$. Taking the slope of the initial linear decrease from Fig. 6 ($|\frac{\Delta T_c}{\Delta x}| = 0.31$ K/%Gd), $\eta_F = 1.65$ states/eV f.u. spin [31], and $S = \frac{7}{2}$ for Gd^{3+} , we estimate $\langle J_{f,s}^2(\mathbf{q}) \rangle^{\frac{1}{2}} = 0.20(7)$ meV. This small value is, presumably, the origin of the significantly extended region of coexistence between superconductivity and magnetism in Fig. 6 and is in agreement with the negligible paramagnetic pair-breaking effects using the Maki parameter (described above).

Similar systems like $La_{1-x}Gd_xAl_2$, $Lu_{1-x}Gd_xNi_2B_2C$, $Y_{1-x}Gd_xNi_2B_2C$, and $La_{1-x}Gd_xSn_3$ present much higher values of the effective exchange interaction, e.g., $\langle J_{f,s}^2(\mathbf{q}) \rangle^{\frac{1}{2}} = 73, 10, 9,$ and 20 meV, respectively, and, as a consequence, a reduced coexistence region of superconductivity and magnetism [32,33]. In general, very low concentrations of magnetic

TABLE II. Generalized simulated annealing ESR parameters obtained for $Y_{1-x}Gd_xPb_3$, Gd content x , $J_{Gd-Gd} \times 10^{-3}$ (meV), b (Oe/K), ΔH_{res} (Oe), and B_4 (Oe).

x	$J_{Gd-Gd} \times 10^{-3}$	b	ΔH_{res}	B_4
0.015	80	2.3	178	40
0.04	42	1.2	118	42
0.07	60	0.6	190	40
0.15	106	0.3	190	41
0.34	550	0.3	432	40

impurities can suppress the superconductivity completely, as in $La_{1-x}Gd_xAl_2$, where $x = 0.003$ of Gd is the critical concentration, strongly contrasting with $Y_{1-x}Gd_xPb_3$, where at $x = 0.15$ of Gd the system still remains a superconductor at about $T_c \sim 3$ K. For samples above this concentration it was not possible to measure T_c due to the broadening of the superconducting transition and the lowest limit of 2 K in our MPMS3 SQUID magnetometer.

This is quite an unusual behavior, wherein significant Gd-Gd magnetic interaction (high negative values for Θ_{CW}) coexists within the same matrix of a superconducting state (inset of Fig. 6). Figure 8 presents the evolution of the Curie-Weiss temperatures for all our samples. Notice the high value for $GdPb_3$ ($\Theta_{CW} = -90$ K), suggesting a significant degree of magnetic frustration ($\Theta_{CW}/T_N = 6.4$).

DFT calculations for YPb_3 [2] reported the presence of p -type (Pb) and d -type (Y) ce at the Fermi level as the main contributions to the density of states and a small contribution of d -type and s -type ce coming from Pb. Since DFT calculations for the isostructural compound YIn_3 lead to similar band structure, we propose that the exchange bottleneck effects observed in [26] in $Y_{1-x}Gd_xIn_3$ may also be present in the $Y_{1-x}Gd_xPb_3$ system, involving the exchange interaction between the Gd^{3+} localized magnetic moment and the s -type ce . In an exchange bottleneck regime the Korringa [20] and Overhauser [34] relaxation mechanisms overcome the ce relaxation to the lattice; then, it may be possible that at high enough Gd^{3+} concentration a simultaneous ce spin-flip scattering of both electrons in a Cooper pair would not result in pair breaking. Notice that an upper limit for the interaction time associated with the exchange interaction between the Gd^{3+} LMM and ce may be evaluated to be $(J/h)^{-1} \sim (0.2 \text{ meV}/h)^{-1} \sim 2 \times 10^{-11}$ s. This hypothesis is strongly supported by our ESR line-shape simulations where the extracted Korringa relaxation rate b is decreasing for high Gd concentrations (see Table II). Within this scenario, assuming that the s -type ce are responsible for the superconductivity, the small value found for the Korringa relaxation rate (extracted from ESR line-shape simulations; see below) may justify the weak decrease of T_c with the Gd concentration. The possibility that different types of ce , like p or d type from Pb, will also be participating in the superconductivity is unlikely due to the strong Gd-Gd coupling, which leads to high negative values of Θ_{CW} , which would then be established by a superexchange-like interaction via p - or d -type ce polarization [15].

A slowing down of the linear decrease rate in T_c at relatively high Gd concentrations similar to our data in Fig. 6 has

already been observed in the $\text{La}_{1-x}\text{Gd}_x\text{Al}_2$ system, and it was attributed to magnetic interactions in which the AG theory cannot be applied. At this point it is important to reiterate that we found no evidence for the presence of Gd clusters in our samples, as evidenced by XRD, SEM images, EDS, and Θ_{CW} measurements. These observations give further support to the idea that, in $\text{Y}_{1-x}\text{Gd}_x\text{Pb}_3$, magnetism is mediated by different types of ce than those mediating the superconductivity.

Figure 9 presents the ESR spectra for powdered crystals of $\text{Y}_{0.985}\text{Gd}_{0.015}\text{Pb}_3$, where a clear Gd^{3+} line narrowing is observed as the temperature increases. Also, the inset shows the narrowing of an estimated overall linewidth at half height of the Gd^{3+} resonance. We associate this narrowing with the exchange narrowing of the Gd^{3+} ESR fine structure [35] due to the Korringa relaxation mechanism. To simulate the narrowing of the Gd ESR powder spectra we use the Plefka-Barnes model [18,19] with an overall linewidth $\Delta H = \Delta H_{\text{res}} + bT$, with b being the Korringa relaxation parameter and ΔH_{res} being the residual linewidth (see Table II). Since the observed ESR spectra are Gd concentration dependent (see Fig. 10), the spin-spin interaction between Gd ions $J_{\text{Gd-Gd}}$ should be relevant (see Table II). We have included this interaction phenomenologically following the procedure of Urban *et al.* [36]. Given the random distribution of Gd ions, we used a distribution of exchange fields for the spin-spin interaction with a mean exchange field of 0.035 Oe and a distribution width of ~ 100 Oe. For the ESR spectra fitting we used a hybrid method that includes least-squares and generalized simulated annealing methods [37]. The simulated line shape, within the temperature range of the experiment for our lowest Gd concentration sample, is presented in Fig. 9 (red line), giving a small Korringa relaxation ($b = \frac{d(\Delta H)}{dT} = 2.3 \text{ Oe/K}$) responsible for the coalescence of the fine structure into a single line of Dysonian-like shape [38]. This approach has thus allowed accurate simulation of spectra line shapes and the system ESR parameters.

Finally, the Korringa relaxation parameter is related to the effective exchange interaction as follows [39]:

$$b = \frac{d(\Delta H)}{dT} = \frac{\pi k_B}{g\mu_B} \langle J_{fs}^2(\mathbf{q}) \rangle \eta_F^2. \quad (2)$$

Then, using the value of b obtained from our ESR line-shape simulations for our lowest Gd concentration, we estimate $\langle J_{fs}^2(\mathbf{q}) \rangle^{\frac{1}{2}} = 3.0(1) \text{ meV}$. This value is larger than that obtained using the AG formalism (T_c vs % Gd). However, it is important

to mention that, in order to obtain good fittings of the ESR line shapes for the various Gd concentration samples, the extracted values for the b parameter were found to be between 0.3 and 2.3 Oe/K (see Table II), and this range is compatible with the small exchange value of 0.20(7) meV obtained from the AG theory. If better and/or larger single crystals of $\text{Y}_x\text{Gd}_{1-x}\text{Pb}_3$ had been available, better resolved ESR spectra could have been obtained, and more consistent values of the Korringa relaxation parameter could have been evaluated.

V. CONCLUSIONS

In summary, our complementary experimental results of superconductivity and Gd^{3+} ESR allow us to conclude that $\text{Y}_{1-x}\text{Gd}_x\text{Pb}_3$ is a system where superconductivity and magnetism coexist within a large concentration region of Gd^{3+} ions. The small experimental value of the effective exchange parameter $\langle J_{fs}^2(\mathbf{q}) \rangle^{\frac{1}{2}} = 0.20(7) \text{ meV}$, obtained from the AG theory, reveals a weak coupling of the Gd^3 ions with the s -type ce , which we argue are responsible for the superconductivity in this material. However, within the accuracy of the ESR experiments and line-shape simulations, this value is in reasonable agreement with those obtained from the ESR line-shape analysis based on the narrowing of the fine structure via a Korringa relaxation mechanism. In spite of the small value obtained for the exchange interaction between Gd^{3+} and s -type ce , J_{fs} , there is evidence for a strong Gd-Gd coupling due to the high Curie-Weiss temperatures found for this system. Thus, this spin-spin-like interaction should be driven by an effective Gd-Gd ce polarization coupling J_{eff} , likely due to a superexchange type of interaction mediated by the presence of different types of ce at the Fermi level, presumably p (Pb) and/or d (Y) [15]. In conclusion, we suggest that superconductivity and magnetism are mediated by different types of ce in $\text{Y}_{1-x}\text{Gd}_x\text{Pb}_3$, allowing the coexistence of these two antagonistic phenomena.

ACKNOWLEDGMENTS

This work was supported by the Brazilian agencies FAPESP (Grants No. 2016/15780-0 and No. 2011/19924-2), CNPq (Grant No. 479541/2013-2), FINEP, and CAPES. The authors are grateful to the Multiuser Central Facilities (UFABC) for the experimental support.

-
- [1] R. Swetarekha, V. Kanchana, A. Svane, S. B. Dugdale, and N. E. Christensen, *J. Phys.: Condens. Matter* **25**, 155501 (2013).
 - [2] J. A. Abraham, G. Pagare, and S. P. Sanyal, *Indian J. Mater. Sci.* **2015**, 296095 (2015).
 - [3] D. Aoki, Y. Katayama, R. Settai, N. Suzuki, K. Sugiyama, K. Kindo, H. Harima, and Y. Ohnuki, *J. Phys. Soc. Jpn.* **67**, 4251 (1998).
 - [4] S. B. Dugdale, *Phys. Rev. B* **83**, 012502 (2011).
 - [5] E. E. Havinga, *Phys. Lett.* **28A**, 350 (1968).
 - [6] E. E. Havinga, H. Damsma, and M. H. van Maaren, *J. Phys. Chem. Solids* **31**, 2653 (1970).
 - [7] D. Endoh *et al.*, *J. Phys. Soc. Jpn.* **58**, 940 (1989).
 - [8] R. D. Hachens and W. E. Wallace, *J. Solid State Chem.* **3**, 564 (1971).
 - [9] R. Settai, K. Sugiyama, A. Yamaguchi, S. Araki, K. Miyake, T. Takeuchi, K. Kindo, Y. Onuki, and Z. Kletowski, *J. Phys. Soc. Jpn.* **69**, 3983 (2000).
 - [10] A. A. Abrikosov and L. P. Gor'kov, *Sov. Phys. JETP* **12**, 1243 (1961).
 - [11] E. M. Bittar, C. Adriano, C. Giles, C. Rettori, Z. Fisk, and P. G. Pagliuso, *J. Phys.: Condens. Matter* **23**, 455701 (2011).

- [12] P. G. Pagliuso, C. Rettori, S. B. Oseroff, P. C. Canfield, E. M. Baggio-Saitovitch, and D. Sanchez, *Phys. Rev. B* **57**, 3668 (1998).
- [13] C. P. Poole, Jr., *Electron Spin Resonance: A Comprehensive Treatise on Experimental Techniques* (Wiley, New York, 1969).
- [14] C. Rettori, D. Davidov, R. Orbach, E. P. Chock, and B. Ricks, *Phys. Rev. B* **7**, 1 (1973).
- [15] M. Cabrera-Baez, A. Naranjo-Uribe, J. M. Osorio-Guillén, C. Rettori, and M. A. Avila, *Phys. Rev. B* **95**, 104407 (2017).
- [16] G. G. Lesseux, T. M. Garitezi, P. F. S. Rosa, C. B. R. Jesus, S. B. Oseroff, J. L. Sarrao, Z. Fisk, R. R. Urbano, P. G. Pagliuso, and C. Rettori, *J. Phys.: Condens. Matter* **28**, 125601 (2016).
- [17] R. H. Taylor, *Adv. Phys.* **24**, 681 (1975).
- [18] T. Plefka, *Phys. Status Solidi B* **55**, 129 (1973).
- [19] S. E. Barnes, *Phys. Rev. B* **9**, 4789 (1974).
- [20] J. Koringa, *Physica (Amsterdam)* **16**, 601 (1950).
- [21] P. C. Canfield and Z. Fisk, *Philos. Mag.* **65**, 1117 (1992).
- [22] R. A. Ribeiro and M. A. Avila, *Philos. Mag.* **92**, 2492 (2012).
- [23] H. P. Klug, *J. Am. Chem. Soc.* **8**, 1493 (1946).
- [24] D. Aoki and J. Flouquet, *J. Phys. Soc. Jpn.* **81**, 011003 (2012).
- [25] H. A. Boorse, D. B. Cook, and M. W. Zemansky, *Phys. Rev.* **78**, 635 (1950).
- [26] M. Cabrera-Baez, W. Iwamoto, E. T. Magnavita, J. M. Osorio-Guillén, R. A. Ribeiro, M. A. Avila, and C. Rettori, *J. Phys.: Condens. Matter* **26**, 175501 (2014).
- [27] N. R. Werthamer, E. Helfand, and P. C. Hohenberg, *Phys. Rev.* **147**, 295 (1966).
- [28] A. M. Clogston, *Phys. Rev. Lett.* **9**, 266 (1962).
- [29] K. Maki, *Phys. Rev.* **148**, 362 (1966).
- [30] M. Zehetmayer, *Supercond. Sci. Technol.* **26**, 043001 (2013).
- [31] E. E. Havinga and M. H. van Maaren, *Phys. Rep.* **10**, 107 (1974).
- [32] P. F. S. Rosa, C. Adriano, T. M. Garitezi, M. M. Piva, K. Mydeen, T. Grant, Z. Fisk, M. Nicklas, R. R. Urbano, R. M. Fernandes, and P. G. Pagliuso, *Sci. Rep.* **4**, 6252 (2014).
- [33] M. B. Maple, *Phys. B (Amsterdam, Neth.)* **215**, 110 (1995).
- [34] A. W. Overhauser, *Phys. Rev.* **89**, 689 (1953).
- [35] P. A. Venegas, F. A. Garcia, D. J. Garcia, G. G. Cabrera, M. A. Avila, and C. Rettori, *Phys. Rev. B* **94**, 235143 (2016).
- [36] P. Urban, D. Davidov, B. Elschner, T. Plefka, and G. Sperlich, *Phys. Rev. B* **12**, 72 (1975).
- [37] C. Tsallis and D. A. Stariolo, *Phys. A (Amsterdam, Neth.)* **233**, 395 (1996).
- [38] F. J. Dyson, *Phys. Rev.* **98**, 349 (1955).
- [39] S. E. Barnes, *Adv. Phys.* **30**, 801 (1981).